Conductance oscillations of a spin-orbit stripe with polarized contacts

M. M. Gelabert[1] and Ll. Serra[1,2]

[1] *Departament de Física, Universitat de les Illes Balears, E-07122 Palma de Mallorca, Spain*
[2] *Institut de Física Interdisciplinar i de Sistemes Complexos IFISC (CSIC-UIB), E-07122 Palma de Mallorca, Spain.*

(Dated: March 30, 2010)

We investigate the linear conductance of a stripe of spin-orbit interaction in a 2D electron gas; that is, a 2D region of length ℓ along the transport direction and infinite in the transverse one in which a spin-orbit interaction of Rashba type is present. Polarization in the contacts is described by means of Zeeman fields. Our model predicts two types of conductance oscillations: Ramsauer oscillations in the minority spin transmission, when both spins can propagate, and Fano oscillations when only one spin propagates. The latter are due to the spin-orbit coupling with quasibound states of the non propagating spin. In the case of polarized contacts in antiparallel configuration Fano-like oscillations of the conductance are still made possible by the spin orbit coupling, even though no spin component is bound by the contacts. To describe these behaviors we propose a simplified model based on an ansatz wave function. In general, we find that the contribution for vanishing transverse momentum dominates and defines the conductance oscillations. Regarding the oscillations with Rashba coupling intensity, our model confirms the spin transistor behavior, but only for high degrees of polarization. Including a position dependent effective mass yields additional oscillations due to the mass jumps at the interfaces.

PACS numbers: 71.70.Ej, 72.25.Dc, 73.63.Nm

I. INTRODUCTION

Spintronics attempts to manipulate the electron spin, alone or in combination with the electron charge, to tune the current in a device or as the bit of information.[1] This novel technology may lead to faster responses and lower power consumptions as compared to the more conventional electronics. A promising approach to spintronics is the control of the spin-orbit interaction, particularly, of the Rashba interaction.[2] This is a spin-orbit coupling due to the lack of inversion symmetry in semiconductor heterostructures, such as those based on InAs or GaAs semiconductors, for which tunability using gate contacts has been demonstrated.[3,4] Exploiting this tunability, Datta and Das proposed the spin field-effect transistor,[5] a ballistic channel between two ferromagnetic leads where current can be manipulated by changing the Rashba strength via an external gate. Despite its simplicity, the limitations of the physical system[6] and of the ballistic transport[7] proved to be long-time obstacles to realizing this device. A recent experiment, however, has overcome these problems demonstrating the feasibility of the Datta-Das transistor.[8]

The Rashba Hamiltonian is composed of two spin-dependent terms; one conserves the longitudinal momentum while the other couples longitudinal and transverse momenta. They are usually called precession and mixing terms, respectively. The mixing term is not present in ideal 1D Datta-Das transistors. More realistic quasi-1D systems are usually considered including a confinement in the transverse direction to transport. The quantum wire with homogeneous spin orbit interaction has been discussed, for instance, in Refs. 9–11. In a similar quantum wire configuration but with the Rashba coupling restricted to a finite region of the wire, recent works showed the importance of the mixing term in the modulation of the conductance.[12–16] These modulations are examples of Fano resonances due to the coupling with quasi bound states. Since this behavior is caused by the spin-orbit coupling alone it has been called the Fano-Rashba effect.[14]

The lateral dimension of the transport channel in the experiments by Koo *et al.*[8] was several microns, which indicates a high degree of 2D character, thus deviating from the 1D or quasi-1D regimes. The quasi-1D multichannel case with polarized contacts was considered in Refs. 17–19 while the 2D system, without confinement in the transverse direction, has been also addressed in Refs. 20–25. In most cases sharp transitions between the contacts and the channel are assumed and matching of the wave functions at the interfaces is the required condition. As an alternative, our approach assumes smooth transitions and describes transmission and reflection between contacts and channel from the numerical wave function, solution of the complete Schrödinger equation. Our purpose is to provide additional insight on the origin and characteristics of different types of conductance oscillations.

In this work we extend the analysis of Ref. 19 to the case of vanishing transverse confinement. We thus focus our interest in a two dimensional electron gas (2DEG) with a stripe of spin-orbit interaction. Polarization in the contacts is modeled by means of effective Zeeman fields, treating the cases of parallel and antiparallel polarizations in arbitrary directions. We assume these Zeeman fields in the contacts are the stray fields of nearby ferromagnets deposited on top of the 2DEG.[26] The direction of the Zeeman field is modeling the orientation of the ferromagnet for each contact. In particular, we are interested in parallel and antiparallel orientation of the

ferromagnets in the plane of the nanostructure. The linear conductance of our model system displays two kinds of oscillations: Ramsauer oscillations when the two spins are propagating and Fano oscillations when only one spin can propagate while the other one is evanescent. Looking at the evolution of the linear conductance with the Rashba coupling intensity, our model confirms the Datta-Das oscillation of the conductance, but only for high degrees of polarization in the contacts.

This paper is organized as follows. In Sec. II we describe the physical system and the model for the current and linear conductance. Section III discusses the dependence of the conductance on energy while the Datta-Das transistor configuration is studied in Sec. IV. In Sec. V we study how the results are affected by a position dependent effective mass. Finally, Sec. VI presents our conclusions.

II. PHYSICAL SYSTEM AND MODEL

We consider a semiconductor 2DEG in the xy-plane with a region of Rashba spin-orbit interaction shaped like an infinite stripe of width ℓ oriented along y. Figure 1a shows a sketch of the physical system. Transport is along x and the asymptotic leads (contacts) are assumed to be spin polarized along a given direction $\hat{n}$. The system Hamiltonian reads

$$\begin{aligned}\mathcal{H} &= -\frac{\hbar^2}{2m_0}\left(\frac{d^2}{dx^2}+\frac{d^2}{dy^2}\right) \\ &+ \Delta(x)\,\hat{n}\cdot\vec{\sigma} + |\Delta(x)| + \mathcal{H}_R, \end{aligned} \tag{1}$$

where $\mathcal{H}_R$ is the Rashba Hamiltonian,

$$\mathcal{H}_R = \frac{1}{\hbar}\left(\alpha(x)p_y\sigma_x - \frac{1}{2}\{\alpha(x),p_x\}\sigma_y\right)\ . \tag{2}$$

Polarized leads in the direction of $\hat{n}$ are described by means of a Zeeman field $\Delta(x)$ that couples to the spin vector $\vec{\sigma}$. A positive scalar potential $|\Delta(x)|$ is also introduced in order to align the majority spin potentials in the contacts with the potential bottom of the central region. This eliminates the effect of a potential mismatch for this spin component and, in practice, it would correspond to use a potential gating of the central region. In Eq. (1) the functions determining the Hamiltonian are $\Delta(x)$ and $\alpha(x)$. These quantities take a constant value in the three parts of our system: left contact (L), central region and right contact (R), and they vary smoothly, described by a Fermi-type function, at the interfaces. See Appendix A for the precise definitions.

We denote by m_0 the conduction-band effective mass of the semiconductor and by α_0 the Rashba intensity of the central region. The Zeeman field in contact c, where $c = L, R$, is denoted by Δ_c, respectively. The case of parallel polarized contacts (P) corresponds to $\Delta_L = \Delta_R \equiv \Delta_0$, while the case of antiparallel polarizations (AP) corresponds to $\Delta_L = -\Delta_R \equiv \Delta_0$, where

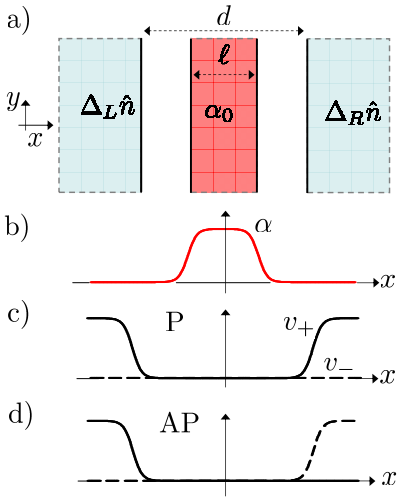

FIG. 1: (Color online) Sketch of the physical system (a) and of the spatial variation of Rashba intensity $\alpha(x)$ (b) and of the spin-dependent potentials $v_\pm(x)$ (c,d). See Sec. II.

Δ_0 is half of the absolute Zeeman splitting. For simplicity, Δ_0 is assumed equal in both contacts. We use the notation $\hat{n}$P and $\hat{n}$AP to indicate parallel and antiparallel configurations along a certain direction $\hat{n}$. Figure 1b shows the variation of the Rashba intensity $\alpha(x)$. It also shows the potentials v_s, for $s = \pm$ spins, defined as

$$v_s(x) = s\Delta(x) + |\Delta(x)|\ . \tag{3}$$

Notice that in the P configuration the $s = -$ spin sees no potential at all while $s = +$ is confined by a potential well of width d. On the contrary, in the AP configuration both spins feel a potential step, but in opposite contacts. As we will discuss below, these differences in potential landscape for $+$ and $-$ spins greatly influence the transport properties of the stripe with polarized contacts.

Typical values of the spin-orbit intensity for InAs based semiconductors can be tuned around $\alpha_0 \approx 10\,\text{meV nm}$, with about one order of magnitude range. Assuming a system length of $\ell \approx 1\,\mu$m and a Zeeman splitting of $\Delta_0 \approx 0.3$ meV this implies that, in adimensional units, one has $\alpha_0 \approx 0.3\sqrt{\hbar^2\Delta_0/m_0}$ and $\ell \approx 10\sqrt{\hbar^2/m_0\Delta_0}$. Having in mind these orders of magnitude we shall explore the variation with energy, for energies around the Zeeman gap, and for Rashba coupling intensities around 0.5 in adimensional units.

Asymptotically, in the 2D contacts, the Hamiltonian eigenfunctions factorize as a plane wave times a spinor in the direction of $\hat{n}$,

$$\Phi_{cs}(\vec{r},\eta;\vec{\kappa}_{cs}) = \exp\left(i\vec{\kappa}_{cs}\cdot\vec{r}\right)\chi_s(\eta)\ , \tag{4}$$

where $c = L, R$ and $s = \pm$ are labelling contact and spin, respectively. The wavenumber $\vec{\kappa}_{cs} \equiv (k_{cs}, q_{cs})$ is composed of the longitudinal (k_{cs}) and transverse (q_{cs}) components. Anticipating a result emphasized below, we note that the transverse momentum is a good quantum

number of the system Hamiltonian, Eq. (1). Therefore, q_{cs} must be a characteristic of the wave function not only in an asymptotic region c and for a given spin s, but throughout the system, i.e., $q_{cs} \equiv q$. At a given Fermi energy E we then have

$$\kappa_{cs}^2 = k_{cs}^2 + q^2 = \frac{2m_0}{\hbar^2}(E - s\Delta_c - |\Delta_c|). \qquad (5)$$

The physically acceptable wave functions fulfill Schrödinger's equation

$$(\mathcal{H} - E)\Psi = 0. \qquad (6)$$

A most general wave function can be taken as a sum on spins and over all transverse momenta (an integral in q)

$$\Psi(\vec{r},\eta) = \sum_{s=\pm} \int dq\, \psi_{qs}(x)\, e^{iqy}\, \chi_s(\eta)\ , \qquad (7)$$

where the unknown functions $\psi_{qs}(x)$ can be interpreted as the wave amplitudes in each channel given by (qs). Projecting Eq. (6) we obtain the channel amplitude equations

$$\left(-\frac{\hbar^2}{2m_0}\frac{d^2}{dx^2} + \frac{\hbar^2 q^2}{2m_0} + v_s(x) - E\right)\psi_{qs}(x) + \sum_{s'=\pm}\left\{\left(\alpha(x)q\langle s|\sigma_x|s'\rangle + \frac{i}{2}\alpha'(x)\langle s|\sigma_y|s'\rangle\right)\psi_{qs'}(x) + i\alpha(x)\langle s|\sigma_y|s'\rangle\frac{d}{dx}\psi_{qs'}(x)\right\} = 0. \qquad (8)$$

Notice that the channel equations for different q's are uncoupled due to the translational invariance of the system in the transverse direction. At a given q, however, the two spin components do couple with each other due to the Rashba spin-orbit interaction. This coupling is described in Eq. (8) by the matrix elements $\langle s|\sigma_{x,y}|s'\rangle$ which can not be diagonalized simultaneously. For any orientation of the spin quantization axis $\hat{n}$, therefore, there is a Rashba-induced interference of the two spin projections. In the contacts the Rashba coupling vanishes and the wave function recovers the good spin eigenstates Φ_{cs} given in Eq. (4).

Integration of Eq. (8) determines the transmission $T_{s's}$, which represents an electron entering the system from the left contact with spin s and going to the right lead with spin s'. It also gives $T'_{s's}$, i.e., from the right contact with spin s to the left one with spin s'. In terms of these transmissions the total current I_x, per unit of length in the transverse direction L_y, can be obtained by adding up the contributions of all electrons in each contact,[27]

$$\frac{I_x}{L_y} = \frac{e}{(2\pi)^2}\int_{k>0} d^2\kappa\, \frac{\hbar k}{m_0}\sum_{ss'} f^{(+)}_{Ls}(\vec{\kappa})\, T_{s's}(\vec{\kappa}) + \frac{e}{(2\pi)^2}\int_{k<0} d^2\kappa\, \frac{\hbar k}{m_0}\sum_{ss'} f^{(-)}_{Rs}(\vec{\kappa})\, T'_{s's}(\vec{\kappa})\ . \qquad (9)$$

In Eq. (9), $f^{(\pm)}_{cs}(\vec{\kappa})$ represents the distribution function of electrons in contact c with spin s, with the upper index indicating right (+) or left (−) direction of motion of the corresponding electron. The distribution of electrons in each contact is given by a Fermi function, characterized by a given chemical potential μ_c. In the linear response regime the bias $\delta V = \mu_R - \mu_L$ is very small and it is enough to retain the linear conductance $I_x = G\delta V$. From Eq. (9) we find the conductance per unit of transverse length

$$\frac{G}{L_y} = \frac{G_0}{4\pi}\sum_{ss'}\left\{\kappa_{Ls}\int_{-\pi/2}^{\pi/2} d\theta\, |\cos\theta|\, T_{s's}(\kappa_{Ls},\theta) + \kappa_{Rs}\int_{\pi/2}^{3\pi/2} d\theta\, |\cos\theta|\, T'_{s's}(\kappa_{Rs},\theta)\right\}\ , \qquad (10)$$

where $G_0 = e^2/h$ is the conductance quantum and κ_{cs} is the Fermi wavevector in contact c, given by Eq. (5) when E is the corresponding Fermi energy.

III. RESULTS

A. Numerical energy dependence

Figures 2 and 3 show typical results obtained numerically from Eq. (10) for x- and y-polarized contacts, respectively. The case of polarization along z is similar to the x one. For each direction (x and y) we also compare the situation of parallel and antiparallel Zeeman fields in the contacts.

For a vanishing Rashba field the transmissions can be obtained analytically. If, in addition to $\alpha_0 = 0$, the Zeeman fields also vanish ($\Delta_0 = 0$), the transmissions trivially become one and the exact conductance is then

$$G = G_0\frac{2}{\pi}\sqrt{\frac{2m_0E}{\hbar^2}}\ . \qquad (11)$$

When $\Delta_0 \neq 0$ we have to distinguish P and AP configurations. The P case is characterized by a perfect transmission of the − spin, while the + spin feels the v_+ potential of Fig. 1. Therefore, its transmission switches on only when $E > 2\Delta_0$. When this occurs, the underlying potential well makes the transmission of the + spin oscillate with energy, even with vanishing spin-orbit. Following Ref. 17, we call these variations Ramsauer oscillations, in analogy with the Ramsauer effect in electron scattering.[28] The importance of these oscillations was pointed out in Ref. 20. Notice also that with vanishing Rashba field the results for x and y orientations of the Zeeman fields are identical.

The energy $2\Delta_0$ signals the transition threshold from only one propagating spin when $E < 2\Delta_0$, to both spins when $E > 2\Delta_0$. At $\alpha_0 = 0$, the P conductance below threshold is given by a pure square root behavior, as in Eq. (11), while above threshold it shows Ramsauer

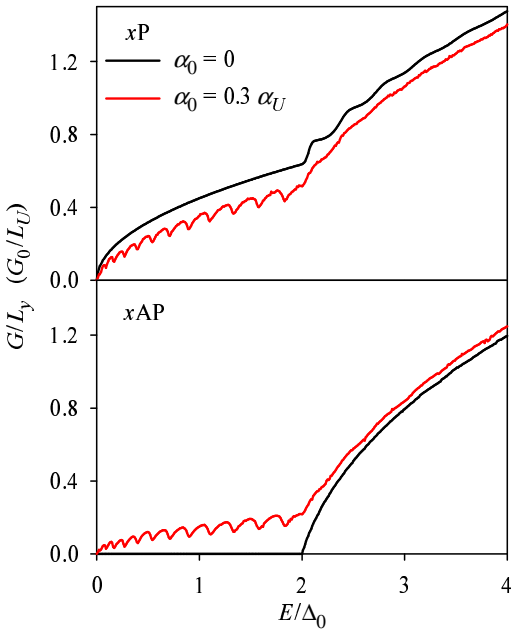

FIG. 2: (Color online) Conductance as a function of energy for polarized contacts along x in P (upper) and AP (lower) configurations. Gray (red in color) and black curves are the results with and without Rashba stripe, respectively. The Zeeman field parameter Δ_0 is taken as energy unit and, accordingly, $L_U = \sqrt{\hbar^2/m_0\Delta_0}$ as length unit. The unit of Rashba coupling intensity is given by $\alpha_U = \sqrt{\hbar^2\Delta_0/m_0}$. Other Hamiltonian parameters: $d = 20\,L_U$, $\ell = 8\,L_U$, $\sigma = 0.1\,L_U$.

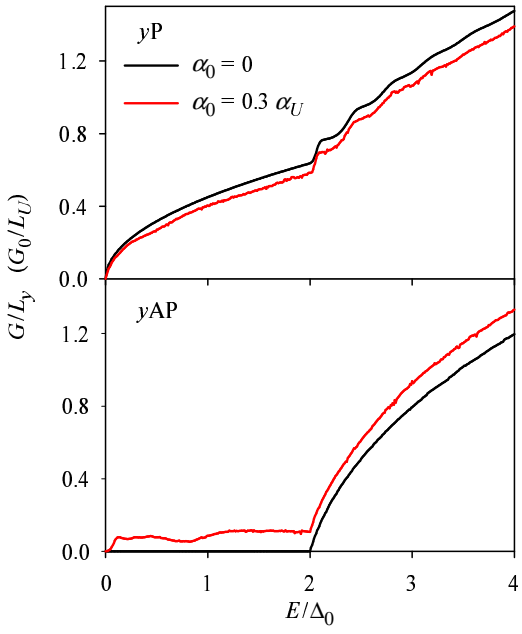

FIG. 3: (Color online) Same as Fig. 2 for polarization of the contacts along y.

oscillations of the minority spin transmission. The AP transmission is exactly zero below threshold ($\alpha_0 = 0$) and above it begins to increase smoothly, as expected for a spin valve. Note that the Ramsauer effect is not active in the AP configuration since the underlying potential is a step, instead of a well.

Turning now to the spin orbit effects, the most conspicuous one is that for $E < 2\Delta_0$, when the contacts are fully polarized, the Rashba field induces the appearance of oscillations in the xP and xAP configurations (Fig. 2). As we will discuss in detail in the next subsection, these oscillations are due to resonant Fano interferences between the propagating spin and the quasibound states of the opposite evanescent spin. They are qualitatively similar to the Fano-Rashba interferences discussed in Ref. 14 for quantum wires. Here, however, the quasibound states are caused by the polarized contacts and not by the Rashba field itself. In the y orientation (Fig. 3), the Fano oscillations below threshold are absent, and only some small variation from the vanishing spin-orbit case can be seen. In general, as shown in Figs. 2 and 3, for the P configuration the results with Rashba coupling (gray-red curve) are slightly below the results without spin-orbit (black curve); while For the AP configuration the situation is reversed.

B. The ansatz model

Let us focus our attention on the oscillations that appear in the fully-polarized-current case, when $E < 2\Delta_0$, both in parallel and antiparallel configurations. The upper panel of Fig. 4 shows the transmission for vanishing transverse momentum in xP configuration, in comparison with the total transmission obtained by integrating over angle θ in Eq. (10). We clearly see that the oscillations in G are due to the deep minima in the transmission for $q = 0$. Besides, the position of these minima coincide with the energies of the bound states in the v_+ potential (dashed lines). At finite q's, not shown in the figure, the transmission minima are shifted or they can even disappear. Physically, we indeed expect the $q = 0$ contribution to dominate the conductance since in this case all the available energy is used in the longitudinal wavenumber. The present transmission minima are examples of Fano resonances due to the interference with quasibound states. To better understand this behavior this subsection presents a simplified model involving the quasibound states in an explicit way.

Assuming $q = 0$ and xP configuration Eq. (8) transforms to

$$\left(-\frac{\hbar^2}{2m_0}\frac{d^2}{dx^2} - E\right)\psi_- = V_m\psi_+\,, \qquad (12)$$

$$\left(-\frac{\hbar^2}{2m_0}\frac{d^2}{dx^2} + v_+ - E\right)\psi_+ = -V_m\psi_-\,, \qquad (13)$$

where we have defined the gradient-dependent mixing potential $V_m \equiv \alpha'(x)/2 + \alpha(x)d/dx$. Equations (12) and (13) constitute a two-channel model, where ψ_- is prop-

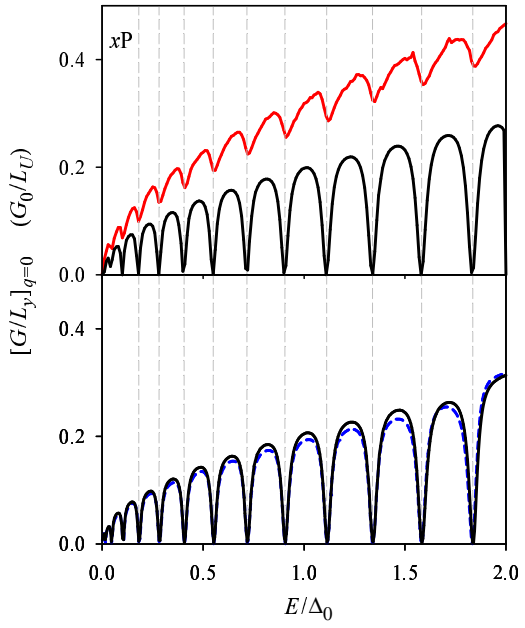

FIG. 4: (Color online) Contribution with $q = 0$ to the linear conductance G/L_y. The vertical dashed lines signal the bound-state energies of the v_+ potential. Except for $\alpha_0 = 0.1\,\alpha_U$, we have used the same parameters and units of Fig. 2. **Upper panel**: $q = 0$ conductance from Eq. (10). For comparison, the gray (red) curve shows the full G/L_y of Eq. (10). **Lower panel**: $q = 0$ conductance from the ansatz model. Solid and dashed lines are from Eqs. (20) and (21), respectively.

agating while ψ_+ is evanescent, with a localized mixing described by V_m. Similar models were obtained for impurities in quantum wires, where semianalytical solutions were worked out using Green functions[29] or the ansatz by Nockel and Stone.[30]

Following Ref. 30 let us make the following ansatz for the evanescent channel amplitude

$$\psi_+(x) = \sum_n A_n\,\phi_n(x)\ , \tag{14}$$

where the A_n's are constants and the ϕ_n's are the bound state wave functions obtained by neglecting interchannel mixing in Eq. (13)

$$\left(-\frac{\hbar^2}{2m_0}\frac{d^2}{dx^2} + v_+ - \varepsilon_n\right)\,\phi_n = 0\ . \tag{15}$$

Notice that if V_m is also neglected in Eq. (12) the propagating channel corresponds to a free particle in 1D. Then, in terms of the free-particle Green function, we may write the general solution of Eq. (12)

$$\psi_- = e^{ikx} + \frac{m_0}{i\hbar^2 k}\int_{-\infty}^{\infty} dx' e^{ik|x-x'|}\,[V_m\psi_+]_{x'}\ , \tag{16}$$

where $k = \sqrt{2m_0E}/\hbar$ and $[V_m\psi_+]_{x'}$ denotes the action of the gradient-dependent potential on ψ_+ at point x'.

Using now the ansatz (14) in Eq. (16), substituting in Eq. (13) and projecting on the set of bound states $\{\phi_n, n = 1,\ldots,N_b\}$ we obtain a matrix equation for the A_n's

$$\sum_{n_2=1}^{N_b}\left[(\varepsilon_{n_1} - E)\delta_{n_1n_2} - \mathcal{M}_{n_1n_2}\right]\,A_{n_2} = \mathcal{B}_{n_1}\ , \tag{17}$$

where

$$\mathcal{M}_{n_1n_2} = \frac{m_0}{i\hbar^2 k}\times \int dx_1dx_2[V_m\phi_{n_1}]_{x_1}[V_m\phi_{n_2}]_{x_2}e^{ik|x_1-x_2|}\ , \tag{18}$$

and

$$\mathcal{B}_{n_1} = \int dx\,[V_m\phi_{n_1}]_x\,e^{ikx}\ . \tag{19}$$

Taking the limit $x \to \infty$ in Eq. (16) we find the amplitude of the transmitted wave

$$t = 1 + \frac{m_0}{i\hbar^2 k}\sum_n A_n\mathcal{B}_n^*\ , \tag{20}$$

and the corresponding transmission $T = |t|^2$. The solid line in Fig. 4 lower panel displays numerical results obtained by solving the matrix equation (17), showing clear transmission minima when the energy is close to a bound state. A more explicit role of the bound states can be seen neglecting nondiagonal terms of the matrix $\mathcal{M}$. In this case, the transmission amplitude reads

$$t = 1 + \frac{m_0}{i\hbar^2 k}\sum_n \frac{|\mathcal{B}_n|^2}{\varepsilon_n - E - \mathcal{M}_{nn}}\ . \tag{21}$$

When $E \approx \varepsilon_n$ the denominator in the right hand side of Eq. (21) reaches a minimum, thus yielding the mechanism by which the bound states produce deep minima in transmission. Notice also that $\mathcal{M}_{nn}$ plays the role of a complex "self energy" that slightly distorts the position of the minima. Nevertheless, displacements of the dips from the bound state energies are hardly seen for weak Rashba couplings since $\mathcal{M}_{nn} \approx \alpha_0^2$. It can also be shown that the relation $\mathrm{Im}\,(\mathcal{M}_{nn}) = -m_0|\mathcal{B}_n|^2/\hbar^2 k$ is fulfilled and that this implies an exactly vanishing conductance at the dip energies.

In the AP configuration no potential well explicitly appears in the Hamiltonian, as shown is the lower panel of Fig. 1. Nevertheless, the results of Fig. 2 prove that the xAP configuration also shows clear oscillations, with conductance dips in similar positions to the xP-polarized case. We can explain this quasibound states as a result of the combination of two effects: a) the reflection on the potential steps in v_+ and v_-; and b) the Rashba induced spin flip. Indeed, adequately combined, the reflection and the spin flip may lead to a trapped state of the electron. Mathematically, we could describe this mechanism

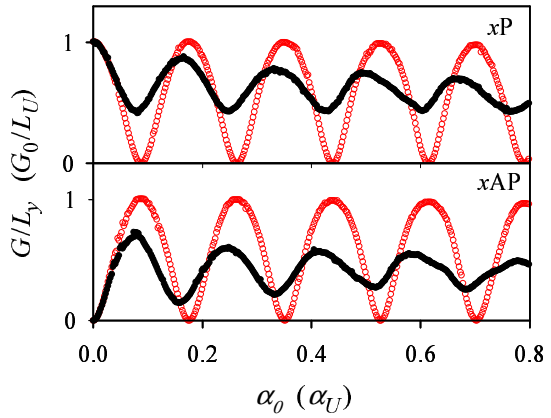

FIG. 5: (Color online) Conductance as a function of Rashba coupling intensity for polarization along x in P and AP configurations. Solid and open symbols are, respectively, the results with and without the Rashba mixing term $\alpha(x)p_y\sigma_x$ of Eq. (2). Differently to the preceding figures, we take here the Fermi energy E as energy unit, with a corresponding length unit $L_U = \sqrt{\hbar^2/m_0 E}$. The Rashba-coupling unit is then $\alpha_U = \sqrt{\hbar^2 E/m_0}$. The remaining system parameters are: $d = 20\sqrt{5}\,L_U$, $L = 8\sqrt{5}\,L_U$, $\Delta_0 = 20\,E$.

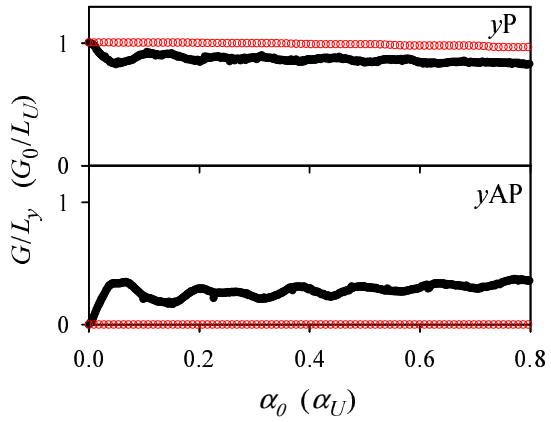

FIG. 6: (Color online) Same as Fig. 5 for polarization along y.

by transforming the Hamiltonian with a local spin rotation $\mathcal{D}(x) = e^{-i\sigma_z\phi(x)}$, where $\phi(x)$ evolves from zero in the left contact to π in the right one. In the transformed problem one component is then effectively bound by the two original potential steps. The transformation is rather cumbersome, however, due to the noncommutation of the kinetic term with $\phi(x)$, in addition to the also noncommuting Pauli matrices.

In the y orientation of the contacts there is no coupling between + and − spins for $q = 0$, as immediately noticed from the term $\alpha(x)q\langle s|\sigma_x|s'\rangle$ of Eq. (8). This explains why there are no clear Fano oscillations for energies below threshold in Fig. 3. The minor features, can be attributed to the Rashba-induced coupling for finite q's.

IV. DATTA-DAS TRANSISTOR

The Datta-Das transistor[5] relies on the oscillatory character of the conductance as a function of the Rashba intensity α_0. In this section we discuss the dependence on α_0, considering first fully polarized contacts ($E < 2\Delta_0$) and, subsequently, partial polarization at the end of the section. The fully polarized results agree overall with other theoretical analysis[22–24] and, qualitatively, with the experiments of Koo *et al.*.[8] Quite surprisingly, however, the oscillatory character of the conductance is rapidly washed out if partial polarization is considered in our model by increasing the energy above the Zeeman threshold $E > 2\Delta_0$.

Figure 5 shows the results of our model for fully polarized leads with spin oriented along x. Upper and lower panels correspond, respectively, to xP and xAP configurations. In each case, solid symbols represent the results for the full Rashba Hamiltonian while open symbols correspond to the neglect of the mixing term. The conductance shows a damped sinusoidal behavior in both cases, with decreasing amplitude as α_0 rises. These results agree with the expected Datta-Das behavior and, therefore, confirm the precession scenario in the continuum 2D case. Similar damped oscillations were obtained in Refs. 22–24. Notice also that this damping is due to the Rashba mixing since it is absent in the open symbols. The oscillation period changes with the distance ℓ and successive minima approximately fulfill the spin precession condition $\ell\alpha_0 = n\pi\hbar^2/m_0$, with $n = 1, 2, \ldots$. In AP configuration the conductance vanishes when $\alpha_0 = 0$ as a consequence of the spin mismatch between both contacts, known as spin-valve behavior. In the presence of Rashba coupling, however, the spin valve behavior is destroyed and we observe that the conductance rapidly increases with α_0, at small couplings, and then oscillates is a similar way to the P case (Fig. 5 lower panel).

For polarized leads along z the results are very similar to those already discussed for polarization along x and, thus, they will not be shown. On the contrary, Fig. 6 corresponds to the configurations along y. Like before, upper and lower panels are for yP and yAP configuration while solid and open symbols represent the cases with and without band mixing, respectively. In this case the conductance oscillations are almost absent, specially in the yP arrangement (upper panel), a result that agrees with the experiments[8] and with the precessing spin scenario.[5] The yP conductance decreases very slowly with α_0 and the effect of mixing is minimal, around a 10% decrease. In yAP orientation we see how the Rashba mixing term again destroys the spin-valve effect at finite α_0's and we observe a small increment in conductance as the Rashba intensity increases. In this configuration there is a reminiscence of the oscillating behavior although much weaker as compared with the x or z orientations.

We turn now to the partially polarized cases, when the energy condition $E > 2\Delta_0$ allows both spins to propagate in the contacts. First notice that the polarization in a

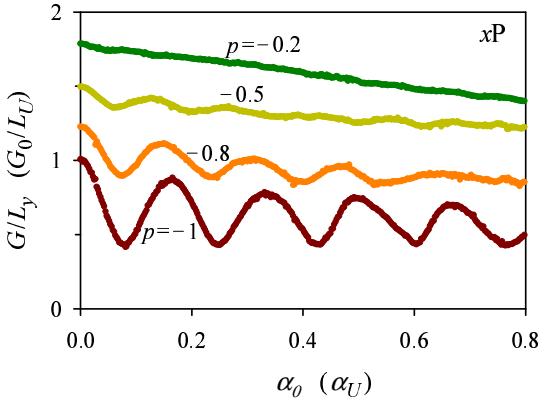

FIG. 7: (Color online) Conductance as a function of α_0 for partial polarizations in xP configuration. The different curves are for varying partial polarizations, from full ($p = -1$) to 20% ($p = -0.2$). Parameters: $d = 20\sqrt{5}\,L_U$, $L = 8\sqrt{5}\,L_U$, units as in Fig. 5.

given contact $c = L, R$ is given by

$$p_c(E,\Delta_c) = \begin{cases} -\dfrac{\Delta_c}{E-|\Delta_c|} & (E \geq 2|\Delta_c|)\ , \\ -\dfrac{\Delta_c}{|\Delta_c|} & (E \leq 2|\Delta_c|)\ , \end{cases} \tag{22}$$

where, as already mentioned in Sec. II, we define (Δ_L, Δ_R) to be (Δ_0, Δ_0) in the P configuration and $(\Delta_0, -\Delta_0)$ in the AP configuration and Δ_0 is assumed positive. The xP results for partial polarizations are presented in Fig. 7. Notice that the oscillatory behavior is greatly quenched when the polarization is decreased, being heavily damped at $|p| = 0.5$ and totally washed out at $|p| = 0.2$. Thus, at low polarizations, our model predicts a monotonous decrease of the conductance with the intensity of the Rashba coupling that is not consistent with the operation of the Datta-Das device.[5] This result shows the importance of having a high degree of polarization in the ferromagnetic contacts for obtaining a robust sinusoidal behavior.

The above results are not substantially modified when using other system parameters, such as changing the energy or the distance between the leads d. The monotonous decrease of the conductance, without oscillations, at low polarizations is also seen in xAP, yP and yAP configurations.

V. SPACE-DEPENDENT EFFECTIVE MASS

In this section we investigate the relevance of having different effective masses in the semiconductor central region and the polarized contacts. Till now the contacts were considered semiconductor materials with a Zeeman field in a given direction. A generalization towards ferromagnetic materials in the contacts has to include the

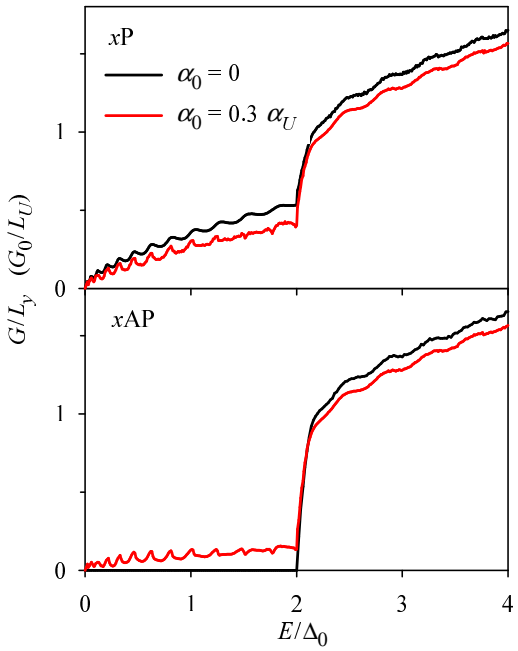

FIG. 8: (Color online) Same as Fig. 2 assuming the effective mass in the contacts is given by $m_c = 15m_0$ ($c = L, R$).

different effective masses of ferromagnet and semiconductor. As in Ref. 31, we then consider the effective mass in the contacs is the bare electron mass m_e while in the central region it is given by the conduction band effective mass of the semiconductor, $0.023m_e$ for InAs and $0.063m_e$ for GaAs. Our aim is not a realistic modeling of ferromagnetic contacts, but to explore the qualitative effects of a position dependent mass on the preceding full semiconductor scenario. In particular, we shall still vary the energy from full to partial polarization, which is not a very realistic assumption for a ferromagnet.

In the spirit of the model, we now use a generalized kinetic term with a position dependent effective mass $m(x)$ (see Appendix A) evolving from the semiconductor mass m_0 in the central region to $15m_0$ in both contacts;

$$T_{\rm kin} = -\frac{d}{dx}\frac{\hbar^2}{2m(x)}\frac{d}{dx} - \frac{\hbar^2}{2m(x)}\frac{d^2}{dy^2}\,. \tag{23}$$

The big jump in effective mass at the interface is smoothed using Fermi functions as explained in Appendix A. The presence of these *effective-mass interfaces* is an additional source of conductance oscillations, as compared to the discussion of the preceding sections. Indeed, in this case even the $\alpha_0 = 0$ conductance with fully polarized contacts displays Ramsauer oscillations, as shown by the black symbols in the upper panel of Fig. 8. Based on the preceding section results, the addition of the spin orbit coupling is expected to introduce new oscillations of Fano type due to the coupling with quasibound states. Surprisingly, both types of oscillations interfere destructively, specially in the vicinity of the polarization threshold $E = 2\Delta_0$, as shown by the gray (red) sym-

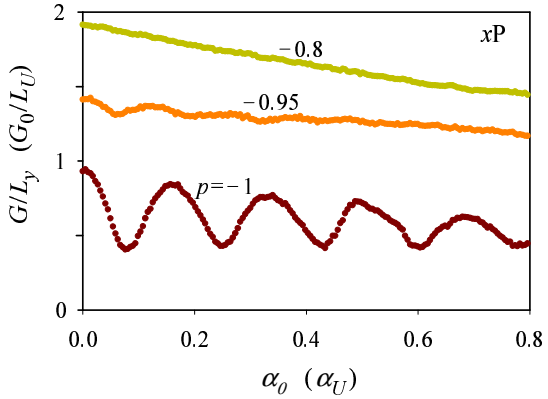

FIG. 9: (Color online) Same as Fig. 7 assuming the effective mass in the contacts is given by $m_c = 15m_0$ $(c = L, R)$.

bols in Fig. 8 upper panel. Another conspicuous effect of the effective mass discontinuity is the big enhancement of conductance when the energy exceeds $2\Delta_0$. This is clearly noticed when comparing the upper panels of Figs 8 and 2.

The lower panel of Fig. 8 shows the xAP conductance with position dependent effective mass. As a difference with Fig. 2 (lower panel), there are Ramsauer oscillations due to the mass jumps for $E > 2\Delta_0$ even for a vanishing α_0. Below threshold we find Rashba-induced oscillations that look very similar to the xP ones in the upper panel. For y oriented contacts the results (not shown), as compared to those of Fig. 3, are also characterized by the appearance of clear Ramsauer oscillations below threshold in the yP configuration while in the yAP orientation the variations are much smaller.

A natural question to ask is whether the effective mass modification affects the conductance oscillations with α_0 discussed in Sec. IV. This is addressed in Fig. 9 for the fully polarized xP configuration. There are small changes, of course, but the overall behavior with damped oscillations is well preserved. Another result we should check is the disappearance of the oscillations at partial polarizations of the contacts (Fig. 7). As proved by Fig. 9, this result is also robust with respect to effective mass changes. Actually, the quenching of the oscillations at partial polarization is enhanced when the mass in the contacts is taken to be the bare mass: already for $|p| < 0.8$ the conductance becomes monotonous, having only a slight decrease with α_0.

VI. CONCLUSIONS

The linear conductance of a 2D stripe of Rashba interaction with polarized contacts behaves in characteristic ways depending on the electron energy, the Rashba intensity as well as on the spin orientation and the degree of polarization of the contacts. We have explored all these degrees of freedom using a single model based on an effective mass approach combined with phenomenological Rashba coupling and Zeeman fields. Our analysis was mostly numerical, in order to avoid additional simplifying assumptions. Nevertheless, semianalytical analysis in terms of coupled channels and quasibound states was also provided.

We have identified two types of oscillations: Ramsauer oscillations due to discontinuities in the effective potential and effective mass; and Fano oscillations due to the coupling with quasibound states. The latter ones are exclusively due to the Rashba coupling. For energies below the full polarization threshold and without mass jumps at the interfaces we obtained pure Fano oscillations in both parallel and antiparallel polarizations along x, while they are absent for polarization along y. With the addition of mass jumps at the interfaces the oscillations are quenched; a result that we attribute to a destructive interference between Fano and Ramsauer oscillations. Above the polarization threshold the conductance displays Ramsauer oscillations in most cases.

Regarding the oscillations in conductance as a function of Rashba coupling, our main result is the rapid quenching of the oscillations when the contacts are partially polarized. This oscillation quenching is even more pronounced when the effective mass increases in the contacts. The oscillations disappear for polarizations below 20% and 80% for constant and position-dependent effective mass, respectively.

Acknowledgments

This work was supported by the MICINN (Spain) Grant FIS2008-00781. Useful discussions with D. Sánchez and R. López are gratefully acknowledged.

Appendix A: Smooth transitions

This appendix contains the precise mathematical forms of the smooth functions $\alpha(x)$, $\Delta(x)$ and $m(x)$ defining the system Hamiltonian. We model the step-like character of these quantities using Fermi functions

$$\mathcal{F}_{x_0,\sigma}(x) = \frac{1}{1 + e^{(x-x_0)/\sigma}} \,, \tag{A1}$$

where x_0 is the position of the step and σ is giving the length around x_0 in which the transition takes place. Precisely, it is

$$\alpha(x) = \alpha_0 \left[\mathcal{F}_{\ell/2,\sigma}(x) - \mathcal{F}_{-\ell/2,\sigma}(x)\right] \,, \tag{A2}$$

$$\Delta(x) = \Delta_L \mathcal{F}_{-d/2,\sigma}(x) + \Delta_R \left[1 - \mathcal{F}_{d/2,\sigma}(x)\right] \,, \tag{A3}$$

$$m(x) = m_L \mathcal{F}_{-d/2,\sigma}(x) + m_R \left[1 - \mathcal{F}_{d/2,\sigma}(x)\right] + m_0 \left[\mathcal{F}_{d/2,\sigma}(x) - \mathcal{F}_{-d/2,\sigma}(x)\right] \,. \tag{A4}$$

where the constants are: α_0, Rashba intensity; Δ_L, Δ_R, Zeeman fields; m_L, m_0 and m_R, effective masses. Notice

that, for the sake of simplicity, we assume a common value for σ in Eqs. (A2), (A3) and (A4).

Appendix B: Resolution method

The numerical calculation of the linear conductance Eq. (10) at a given energy E involves two steps. First, for a certain angle θ, or what is equivalent, a certain transverse momentum q, the coupled equations for ψ_{q+} and ψ_{q-}, Eqs. (8), are solved to obtain the transmissions $T_{s's}$ and $T'_{s's}$. This is accomplished using the transmitting-boundary algorithm as in Ref. 19. The calculation of Ref. 19 was for quantum wires, with a confinement potential in the transverse direction, where the system of coupled equations was infinite and had to be truncated. The present case is, in this respect, simpler since only the two spin components of a given transverse momentum need to be considered. Nevertheless, the reader is addressed to Ref. 19 for the technical details on how the differential equations with open boundary conditions are transformed into a linear system of equations.[32]

Once the transmissions at a fixed θ are obtained, a second step of the calculation requires to integrate over the angle to calculate the linear conductance from Eq. (10). This integral turns out to be somewhat delicate due to the presence of resonances as discussed in the quasi-analytical solution by ansatz of Sec. III.B. The θ-integration is then carried out using Gauss-Legendre quadratures with a certain set of abcissae and weights. To make sure that the integral is well converged we keep increasing the number of Gauss-Legendre points until a required accuracy is reached in a stable way. Typically, we require the error to be $\Delta G/G_0 \leq 10^{-3}$.

[1] J. Fabian, A. Matos-Abiague, C. Ertler, P. Stano, and I. Zutic, Acta Phys. Slov. **57**, 565 (2007).
[2] E. I. Rashba, Fiz. Tverd, Tela (Leningrad) **2**, 1224 (1960). [Sov. Phys. Solid State **2**, 1109 (1960)]
[3] J. Nitta, T. Akazaki, H. Takayanagi, and T. Enoki, Phys. Rev. Lett. **78**, 1335 (1997).
[4] G. Engels, J. Lange, Th. Schäpers, and H. Lüth, Phys. Rev. B **55**, R1958 (1997).
[5] S. Datta and B. Das, Appl Phys. Lett. **56**, 665 (1990).
[6] G. Schmidt, D. Ferrand, L. W. Molenkamp, A. T. Filip and B. J. van Wees, Phys. Rev. B **62**, R4790 (2000).
[7] J. Schliemann, J. C. Egues, and D. Loss, Phys. Rev. Lett. **90**, 146801 (2003).
[8] H. C. Koo, J. H. Kwon, J. Eom, J. Chang, S. H. Han, and M. Johnson, Science **325**, 1515 (2009).
[9] M. Governale and U. Zülicke, Solid State Commun. **131**, 581 (2004).
[10] Ll. Serra, D. Sánchez, and R. López, Phys. Rev. B **72**, 235309 (2005).
[11] C. A. Perroni, D. Bercioux, V. Marigliano Ramaglia, and V. Cataudella, J. Phys.: Condens. Matter **19**, 186227 (2007).
[12] I. A. Shelykh and N. G. Galkin, Phys. Rev. B **70**, 205328 (2004).
[13] L. Zhang, P. Brusheim, and H.Q. Xu, Phys. Rev. B **72**, 045347 (2005).
[14] D. Sánchez and Ll. Serra, Phys. Rev. B **74**, 153313 (2006).
[15] R. López, D. Sánchez and Ll. Serra, Phys. Rev. B **76**, 035307 (2007).
[16] D. Sánchez, Ll. Serra, and M.-S. Choi, Phys. Rev. B **77**, 035315 (2008).
[17] M. Cahay, S. Bandyopadhyay, Phys. Rev. B **68**, 115316 (2003).
[18] J. S. Jeong and H.-W. Lee, Phys. Rev. B **74**, 195311 (2006).
[19] M. M. Gelabert, Ll. Serra, D. Sánchez, and R. López, Phys. Rev. B **81**, 165317 (2010).
[20] T. Matsuyama, C.-M. Hu, D. Grundler, G. Meier, and U. Merkt, Phys. Rev. B **65**, 155322 (2002).
[21] M. Khodas, A. Shekhter, and A. M. Finkelstein, Phys. Rev. Lett. **92**, 086602 (2004); A. Shekhter, M. Khodas, and A. M. Finkelstein, Phys. Rev. B **71**, 125114 (2005).
[22] M. G. Pala, M. Governale, J. König, and U. Zülicke, Europhys. Lett. **65**, 850 (2004).
[23] P. Agnihotri and S. Bandyopadhyay, Physica E **42**, 1736 (2010).
[24] A. N. M. Zainuddin, S. Hong, L. Siddiqui, and S. Datta, arXiv:1001.1523 (unpublished, 2010).
[25] O. Entin-Wohlman, A. Aharony, Y. Tokura, and Y. Avishai, Phys. Rev. B **81**, 075439 (2010).
[26] J. Wróbel, T. Dietl, K. Fronc, A. Lusakowsky, M. Czeczott, G. Grabecki, R. Hey, K. H. Ploog, Physica E **10**, 91 (2001).
[27] D. K. Ferry and S. M. Goodnick, *Transport in nanostructures* (Cambridge, UK, 1997). Sec. 3.3.1.
[28] L. I. Schiff, *Quantum Mechanics* (McGraw-Hill, Singapore, 1985).
[29] S. A. Gurvitz and Y. B. Levinson, Phys. Rev. B **47**, 10578 (1993).
[30] J. U. Nöckel and A. D. Stone, Phys. Rev. B **50**, 17415 (1994).
[31] F. Mireles, G. Kirczenow, Phys. Rev. B **66**, 214415 (2002).
[32] We have used a linear sparse solver from: HSL, A Collection of Fortran codes for large-scale scientific computation. See http://www.hsl.rl.ac.uk, (2007)